e-ISSN:2319-9849
p-ISSN:2322-00

Research & Reviews: Journal of Chemistry

The Effect of Metal-Remote Amino-Groups on Metal Center in Ruthenium (II) Complexes with Terpyridine Ligands

Li H[1], Jeilani YA[2], Melnyczuk JM[1], Hibbard L[2], Wu J[3], Yerokun T[2], Ingram CW[1] and Harruna I[1]*

[1]Chemistry Department, Clark Atlanta University, Atlanta, USA.

[2]Department of Chemistry and Biochemistry, Spelman College, Atlanta, USA.

[3]School of Materials Science and Engineering, Georgia Institute of Technology, Atlanta, USA.

RESEARCH

Received date: 13/07/2015
Accepted date: 16/07/2015
Published date: 21/07/2015

***For Correspondence**

Harruna I, Chemistry Department, Clark Atlanta University, Atlanta, USA

E-mail: iharruna@cau.edu

Keyword: Ruthenium complexes, HOMO-LUMO gap, Terpyridine, DFT calculations.

ABSTRACT

The aim of this work is to study structure, spectra and optical properties of ruthenium complexes with applications in the development of biosensors for cellular imaging. The results showed that a ruthenium complex with 4′-(aminomethylphenyl) -2, 2′: 6′, 2″ terpyridine ($[Ru(TpyCH_2NH_2)_2]^{2+}$) ligand has unique amino groups that reduce the energy gap between the highest occupied molecular orbital (HOMO) and the lowest unoccupied molecular orbital (LUMO). The all ligand-HOMO composition of $[Ru(TpyCH_2NH_2)_2]^{2+}$ is contributed by the amino groups of the $TpyCH_2NH_2$ ligands. In a cell uptake test and proliferation assay, the ruthenium complex with amino group show cytoplasmic location and dose-dependent cytotoxic effect on 647V bladder cancer cells but not the complex with carboxylic as ligand substituent. Both experiment and calculation explore how the amino substituents affect the properties of the complex compared to the simple $[Ru(Tpy)_2]^{2+}$ systems (where Tpy = 2, 2′: 6′, 2″ terpyridine). The HOMO-LUMO energy gap calculation results of $[Ru(TpyCH_2NH_2)_2]^{2+}$ at the B3LYP/LANL2DZ level of theory is consistent with the spectroscopic and electrochemical experimental results.

INTRODUCTION

Fundamental understanding of the metal remote substituent group effect on the properties of organometallic complexes can be used in the rational design of new materials with unique properties [1-3]. In some cases, metal remote functional groups in Ru (II) complexes have been used to functionalize multiwalled carbon nanotubes to enhance electronic resistance of nanotubes [3]. Ruthenium complexes have been found to have potential applications in opto-electronic device and nanotechnology [1-5], development of efficient solar cells [6], and invention of new probes for DNA structure and function [7]. The ultraviolet visible (UV-Vis) spectra of such materials are typically characterized by a metal-to-ligand charge transfer (MLCT) band in the visible region with stability that is generally attributed to the σ-donor / π-acceptor character of a metal–nitrogen bond. These Ru (II) complexes possess various important photophysical features that arise from the population of a triplet luminescent level as the lowest excited-state after photoexcitation [1, 2]. Numerous studies have focused on metallocomplexes with small energy gaps between the highest occupied molecular orbital (HOMO) and the lowest unoccupied molecular orbital (LUMO). One important characteristic of Ru(II) complexes is their small HOMO-LUMO gap. Lowering HOMO-LUMO gap plays an important role in studying electron transfer phenomena and molecular designs [8-9], and controlling the HOMO-LUMO gap is highly desired for opto-electronic device and luminescence [10-16].

The effect of ligands on HOMO-LUMO gap has been reported by density functional theory (DFT) methods [10-16]. A recent study

reported that introducing a carboxylic group to Ru(II) ligands does not change the energy gap of HOMO-LUMO [10-13]; while amine and hydroxyl substituted porphyrins have been reported to lead to smaller HOMO-LUMO gaps [14,16].

In the current study, Ru(II) complexes with functionalized terpyridines were synthesized and the optical properties were evaluated. DFT results show that the presence of amino groups as ligand substituents leads to a lowering energy gap of HOMO-LUMO. The calculations reveal that these two amino groups alter HOMO composition of $Ru(TpyCH_2NH_2)_2^{2+}$. Finally, $[Ru(TpyCH_2NH_2)_2]^{2+}$ shows luminescence and stability for application in cellular imaging.

MATERIALS AND METHODS

MaterialsAll chemicals and solvents used for spectroscopic measurement are of spectroscopic grade and commercially available (Sigma-Aldrich Company). Bladder 647V cells are purchased from American Type Culture Collection, Manassas, VA.

Instruments. ^1H and ^{13}C- NMR spectra were recorded on a Bruker 500 MHz spectrometer; UV-vis spectra were recorded using a Beckman DU640 spectrophotometer in acetonitrile (MeCN). High resolution Mass spectrometry (MALDI-TOF) was performed on a Micromass Tof Spec-2E mass spectrometer. Fourier transform infrared spectrum (FTIR) was measured with a Perkin Elmer spectrum 65 FTIR infrared spectrometer; samples were prepared and compressed in KBr pellet. Fluorescence emission spectra were measured on HORIBA Fluorolog 3-21 spectrometer in acetonitrile (MeCN). Cyclic Voltammogram was measured on a PARSTAT®2263 (Princeton Applied Research Inc). In acetonitrile with a working electrode of Solid Electrode (Working Electrode Area is 1.000 cm^2) and reference electrode of Ag, AgCl / NaCl (sat'd) (0.194V). The whole system is working at room temperature under argon protection. The electrochemical potentials of electrodes are calibrated with respect to a ferrocene and ferrocenium couple. Fluorescence Imaging was performed using the EVOS fluorescent microscope (AMG Co). The electrochemical method is expressed as:

$$I_p = (E_{onset,ox} + 4.4)\ (eV); \quad (1)$$

$$E_a = (E_{onset,\ red} + 4.4)\ (eV); \quad (2)$$

Where I_p is the ionization potential, E_a is electron affinity, $E_{onset,\ ox}$ is the onset potential of oxidation and $E_{onset,\ red}$ is the onset potential of reduction. The HOMO-LUMO energy gap was calculated by Hamiltonian calculation and electrochemical method [8] using Eqs. (1) and (2).

Computational Methods

Density functional theory (DFT) calculations were performed on the Gaussian 09W suite of programs [17, 18]. DFT was used to determine both optimum geometry and energies of the Ru(II) complexes. Four independent density functionals were used: B3LYP [19, 20], X3LYP [21], and B3PW91 [23]. LANL2DZ basis set were used for calculation comparison [24-26]. All optimized geometries were subjected to vibration frequency analysis to ensure they corresponded to potential energy minima without imaginary frequency. Atomic charges and orbital populations were calculated by natural bond orbital analysis (NBO) [17, 27]. Zero point energies were obtained from harmonic vibrational frequency calculations without scaling. The translational, rotational and vibrational contributions to the enthalpy and entropy were evaluated using rigid-rotor and harmonic oscillation approximations. Optimized structures and atomic charges were visualized with the GaussView 4.1 software package [28]. Time-dependent density functional theory (TD-DFT) calculations were performed at the B3LYP/LANL2DZ level to arrive at the vertical singlet excited states for each complex from the corresponding optimized singlet ground state geometry using the PCM model with acetonitrile as the solvent.

Synthesis

A ruthenium (II) bis [4′-(aminomomethylphenyl) -2, 2′:6′, 2″-terpyridine] bi-tetrafluoroborate, i.e. $[Ru(TpyCH_2NH_2)_2](BF_4)_2$, was synthesized according to the literature reported [2,29-30]. To synthesize $[Ru(TpyCH_2NH_2)_2](BF_4)_2$ **(Scheme 1)**, a mixture of $RuCl_3{\cdot}xH_2O$ (0.047 g, 0.18 mmol) and $AgBF_4$ (0.116 g, 0.59 mmol) have been refluxed for 2 hours in 15 ml acetone. After cooling to room temperature, the precipitated AgCl was removed by filtration, the solution was evaporated to afford dark solid powder of $[Ru(III)(Me_2CO)_6](BF_4)_3$. The solid product was then dissolved in 15 ml 1-butanol and $TpyCH_2NH_2$ (0.122 g, 0.36 mmol) was added and refluxed for 12 hours under argon protection. A further portion of $TpyCH_2NH_2$ (0.10 g, 0.026 mmol) was added, and refluxing continued for an additional 12 h. The solution was cooled to room temperature; the solid was filtered off and washed with 1-butanol (100 ml). The final products were obtained after evaporation and dried in vacuum (phosphorus oxide), to yield a dark red solid $[Ru(TpyCH_2NH_2)_2](BF_4)_2$ (yield: 52.2%, 78 mg).

MALDI-TOF-HRMS calculated 777.9004 for $C_{44}H_{36}N_8Ru$ $[M\text{-}NH_2\text{-}2BF_4+H]^+$, found: 778.2952. ^1H NMR (400 MHz, $[D_6]$ DMSO, 25°C, TMS):): δ (ppm) 4.20 (s, 4H; CH2), 7.29 (t, 4H;CHPh), 7.56 (d, 4H; CHPh), 7.85 (t, 4H; CHP), 8.06 (t, 4H; CHPh), 8.50 (d, 4H; CHPh), 9.12(d, 4H; CHPh), 9.51 ppm (s, 4H; CHPh); ^{13}C-NMR (500 MHz, $[D_6]$ DMSO, 25°C) δ(ppm):158.4, 155.6, 152.6, 146.7, 136.9, 136.5, 133.7, 130.1, 128.3, 125.3, 121.5, 42.6. MADIL-TOF-MS: m/z calculated 967.2 for M^+, found 968.2 $[M+H]^+$, 966.2 $[M-H]^+$, 922.2 $[M\text{-}2BF_4\text{-}2NH_2\text{-}CH_2]^+$, 865.2 $[M\text{-}NH_2\text{-}BF_4+H]^+$, 778.2 $[M\text{-}NH_2\text{-}2BF_4+H]^+$. FTIR (KBr, vcm^{-1}) 3403 (s); 3054 (s); 2883 (m); 2834 (m); 1829 (w); 1608 (s); 1583 (s); 1568 (s); 1545(s); 1472(s); 1439(s); 1406 (m); 1390(s); 1088(s); 1055(s); 1027(s); 832(w); 790 (s); 746 (s); 667 (w); 520 (w); 480 (w). UV-VIS (in MeCN): λmax nm (log ε) = 252 (4.25); 276 (4.38); 309 (3.79) and 493 nm (3.09). Elemental Analysis Calculated (%) for $C_{45}H_{39}B_2F_8N_8Ru$; C 55.92; H, 4.07; N, 11.59; Found: C 55.86; H, 4.09; N, 11.62.

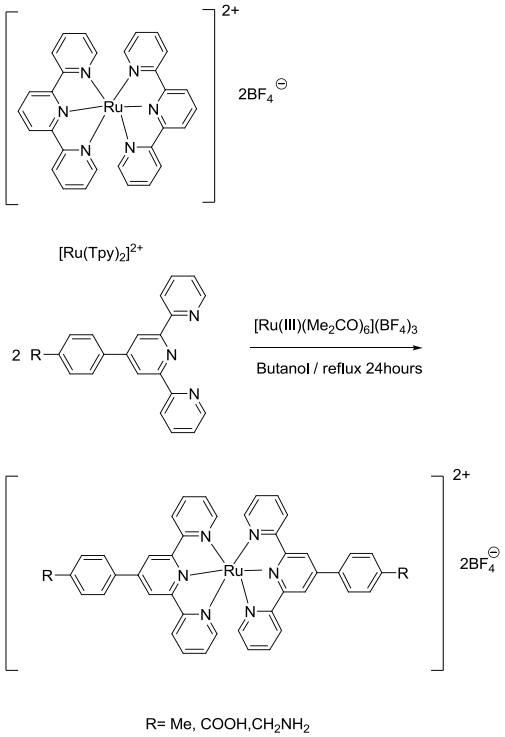

Scheme 1. Synthesis of ruthenium (II) terpyridine complexes and their structures.

Ruthenium (II) bis [4′-(methylphenyl) -2, 2′:6′,2″-terpyridine] bi-tetrafluoroborate; i.e. $[Ru(TpyCH_3)_2](BF_4)_2$ and Ruthenium (II) bis [4′-(carboxylphenyl) -2,2′:6′,2″-terpyridine] bi-tetrafluoroborate, $[Ru(TpyCOOH)_2](BF_4)_2$ were also synthesized with the same procedure. The identified structures were consistent with what is found in literature [31,32]. The purities of all ruthenium complexes were tested before spectroscopy measurements were taken.

Biotest

Bladder 647V cells were grown in F12-K medium supplemented with 10% fetal calf serum, penicillin (100 µg/ml) and streptomycin (100 U/ml), at 37 °C, in a 5% CO_2 atmosphere cell culture incubator. Cells were plated overnight at 5×10^4 cells per well of a 96-well culture plate for the proliferation assay, or in a culture slide for live imaging with a fluorescent microscope. Cells growing near the confluence on culture slides were rinsed with 1× phosphate buffered saline (PBS) and the culture medium replaced with 10 um concentration of the Ru complex dissolved in culture medium without the growth supplement. Live-cells were imaged under the EVOS fluorescent microscope monitored at 488 nm wavelength for fluorescence. Proliferation assay was carried out as follows: cells were incubated at 96-well plates and allowed to acclimatize overnight. They were then incubated in selected Ru complex solution. These were performed in triplicate wells each incubation concentration. After 24 hour incubation at 37°C under 5% CO_2, absorbance reading at 450 nm for each well was used to compute percent proliferation relative to control cells in untreated wells.

RESULTS AND DISCUSSION

Three ruthenium complexes, $[Ru(TpyCH_2NH_2)_2](BF_4)_2$, $[Ru(TpyCH_3)_2](BF_4)_2$ and $[Ru(TpyCOOH)_2](BF_4)_2$ were synthesized according to **Scheme 1**. Their structures were studied by both absorption spectroscopy and density functional theory (DFT) methods. These complexes were evaluated as potential dyes to visualize biological samples. The $[RuTpyCH_2NH_2)_2](BF_4)_2$ complex has unique NH_2 groups, each with a lone pair of electrons that is remote from the Ru center. Structural features of this complex are discussed together with a comparison to the structures of $[Ru(TpyCH_3)_2](BF_4)_2$ and $[Ru(TpyCOOH)_2](BF_4)_2$.

Electronic Structure

The effective atomic charge on Ru was also calculated by NBO [17,27]. The atomic charge calculation is highly dependent on basis sets. With LANL2DZ basis set, the atomic charge on Ru in $[Ru(TpyCH_2NH_2)_2]^{2+}$ ranged between +0.26 and +0.30, using B3LYP, X3LYP, and B3PW91. To test the effects of the basis sets, optimization of the At B3LYP/3-21G level of theory of $[Ru(TpyCH_2NH_2)_2]^{2+}$ gave Ru charge of +0.36. This demonstrates and confirms a small charged on Ru. This small localized charged on Ru, which is significantly lower than the expected +2 charge; that is consistent with a previous study of Ru complexes that led to a similar small charge of +0.46 on Ru [33].

Molecular Orbital Compositions of Ru Complexes

Population analysis at B3LYP/LANL2DZ level of theory was performed to better understand the composition of the frontier

molecular orbital of the Ru complexes. All complexes have degenerate HOMO/HOMO-1 and LUMO/LUMO+1 **(Figure 1 and Table 1)**. The degenerate LUMO and LUMO-1 orbitals of $[RuTpyCH_2NH_2)_2]^{2+}$ are slightly higher in energy than those of $[Ru(TpyCH_3)_2]^{2+}$ and $[Ru(TpyCOOH)_2]^{2+}$ **(Table 1)**. Also, the CH_2-NH_2 group in $[Ru(TpyCH_2NH_2)_2]^{2+}$ makes a significant difference in the composition of HOMO and HOMO-1 with respect to $[Ru(TpyCH_3)_2]^{2+}$ and $[Ru(TpyCOOH)_2]^{2+}$; both HOMO and HOMO-1 of $[Ru(TpyCH_2NH_2)_2]^{2+}$ are composed of 100% ligand orbitals while the contribution of Ru orbitals to the HOMO/HOMO-1 of $[Ru(TpyCH_3)_2]^{2+}$ and $[Ru(TpyCOOH)_2]^{2+}$ is 57% and 36%, respectively **(Figure 1)**. These results show the important role of remote amino groups in Ru complexes by making all-ligand HOMO/HOMO-1.

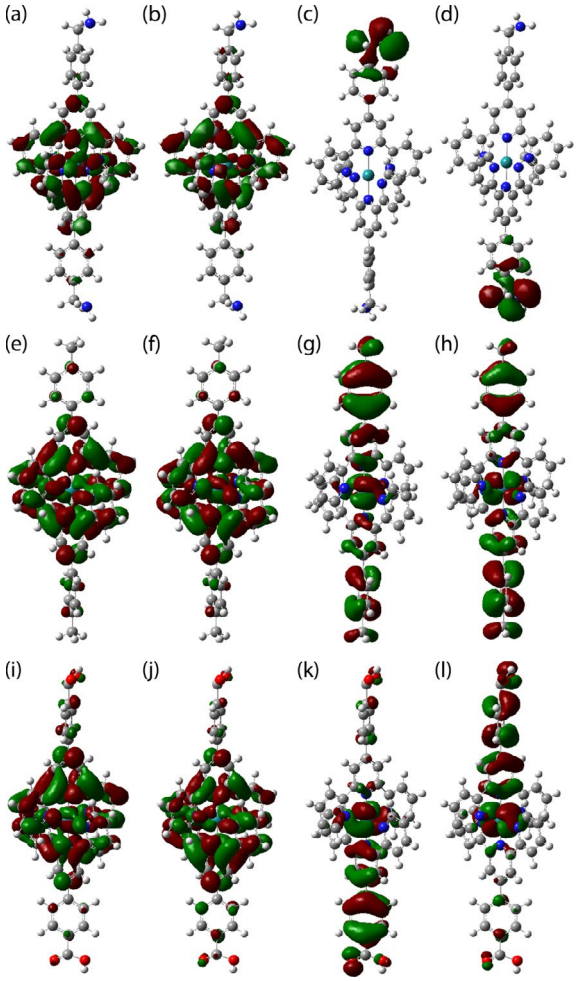

Figure 1. Frontier molecular orbitals: (a) LUMO+1 of $[Ru(TpyCH_2NH_2)_2]^{2+}$, (b) LUMO of $[Ru(TpyCH_2NH_2)_2]^{2+}$, (c) HOMO of $[Ru(TpyCH_2NH_2)_2]^{2+}$, (d) HOMO-1 of $[Ru(TpyCH_2NH_2)_2]^{2+}$, (e) LUMO+1 of $Ru[TpyCH_3]_2^{2+}$, (f) LUMO of $Ru[TpyCH_3]_2^{2+}$, (g) HOMO of $Ru[TpyCH_3]_2^{2+}$, (h) HOMO-1 of $Ru[TpyCH_3]_2^{2+}$, (i) LUMO+1 of $[Ru(TpyCOOH)_2]^{2+}$, (j) LUMO of $[Ru(TpyCOOH)_2]^{2+}$, (k) HOMO of $[Ru(TpyCOOH)_2]^{2+}$, (l) HOMO-1 of $[Ru(TpyCOOH)_2]^{2+}$.

Table 1. Percent Ru in frontier orbitals and orbital energies (eV) of the complexes at the B3LYP/LANL2DZ level of theory

MO #	$[Ru(TpyCOOH)_2]^{2+}$		$[Ru(TpyCH_3)_2]^{2+}$		$[Ru(TpyCH_2NH_2)_2]^{2+}$		$[Ru(Tpy)_2]^{2+}$	
	% Ru	MO # (Energy eV)	% Ru	MO # (Energy eV)	% Ru	MO # (Energy eV)	% Ru	MO# (Energy eV)
LUMO+4	0	196 (-6.556)	0	182 (-6.338)	0	190 (-6.232)	0	174 (-6.431)
LUMO+3	4	195 (-7.334)	4	181 (-7.068)	4	189 (-6.952)	6	173 (-7.179)
LUMO+2	0	194 (-7.422)	0	180 (-7.159)	0	188 (-7.038)	0	172 (-7.269)
LUMO+1	8	193 (-7.576)	8	179 (-7.288)	8	187 (-7.176)	9	171 (-7.403)
LUMO	8	192 (-7.576)	8	178 (-7.288)	8	186 (-7.176)	9	170 (-7.403)
HOMO	57	191 (-10.856)	36	177 (-10.383)	0	185 (-9.471)	53	169 (-10.645)
HOMO-1	57	190 (-10.856	36	176 (-10.383)	0	184 (-9.471)	53	168 (-10.645)
HOMO-2	78	189 (-10.967)	78	175 (-10.704)	34	183 (-10.318)	83	167 (-10.816)
HOMO-3	0	188 (-11.191)	38	174 (-11.026)	34	182 (-10.319)	0	166 (-11.152)
HOMO-4	0	187 (-11.191)	38	173 (-11.026)	78	181 (-10.633)	6	165 (-11.153)

The contributions of Ru orbitals to HOMOs of Ru octahedral complexes have been typically reported [22,23]. Transition metal complexes with no metal contribution in the HOMO have been previously reported [34]. On the other hand, introducing ligands containing amino groups to the complex does not necessarily lead to a Ru complex with HOMOs located around nitrogen atoms

of the ligands; for example, DFT studies of Ru(porphyrin)$(NH_3)_2$ complex showed more Ru contribution to HOMO than the nitrogen atoms of two amino groups [35].

Figure 1 shows that the HOMO-1 and HOMO of $[Ru(TpyCH_2NH_2)_2]^{2+}$ are localized around the NH_2 groups. The contribution of the Ru d-orbitals appear in the HOMO-2 and HOMO-3 of $[Ru(TpyCH_2NH_2)_2]^{2+}$ **(Table 1)**. **Table 1** shows that the contribution of ruthenium d-orbital to LUMO is 8% in $[Ru(TpyCH_2NH_2)_2]^{2+}$, $[Ru(TpyCH_3)_2]^{2+}$ and $[Ru(TpyCOOH)_2]^{2+}$,while the LUMO+2 is an all-ligand molecular orbital in these complexes.

Determination of HOMO-LUMO Gap of the Ruthenium Complexes

The HOMO-LUMO gap plays an important role in the spectroscopic behavior of transition metal complexes. At B3LYP/LANL2DZ level of theory, the HOMO-LUMO energy gaps for $[Ru(TpyCH_2NH_2)_2]^{2+}$, $[Ru(TpyCH_3)_2]^{2+}$, $[Ru(TpyCOOH)_2]^{2+}$, $[Ru(Tpy)_2]^{2+}$ were 2.3, 3.1, 3.3, 3.2 eV, respectively **(Figure 2)**. The use of the 3-21G basis set gave similar results. The $[Ru(TpyCH_2NH_2)_2]^{2+}$ has the lowest HOMO-LUMO energy gap; **Figure 2** shows that the degenerate HOMO/HOMO-1 of $[Ru(TpyCH_2NH_2)_2]^{2+}$ is at a relatively higher energy than the $[Ru(TpyCH_3)_2]^{2+}$ and $[Ru(TpyCOOH)_2]^{2+}$ complexes while the energy level of the LUMOs in these complexes are at relatively comparable energy levels. It appears that the higher energy HOMOs of $[Ru(TpyCH_2NH_2)_2]^{2+}$ leads to the small HOMO/LUMO energy gap. These results indicate that introduction of the CH_2NH_2 group into the terpyridine ligand lowers the HOMO-LUMO gap. For $[Ru(TpyCH_2NH_2)_2]^{2+}$, the calculated HOMO-LUMO energy gap is in good agreement using B3LYP, X3LYP and B3PW91 functionals **(Table 2)**.

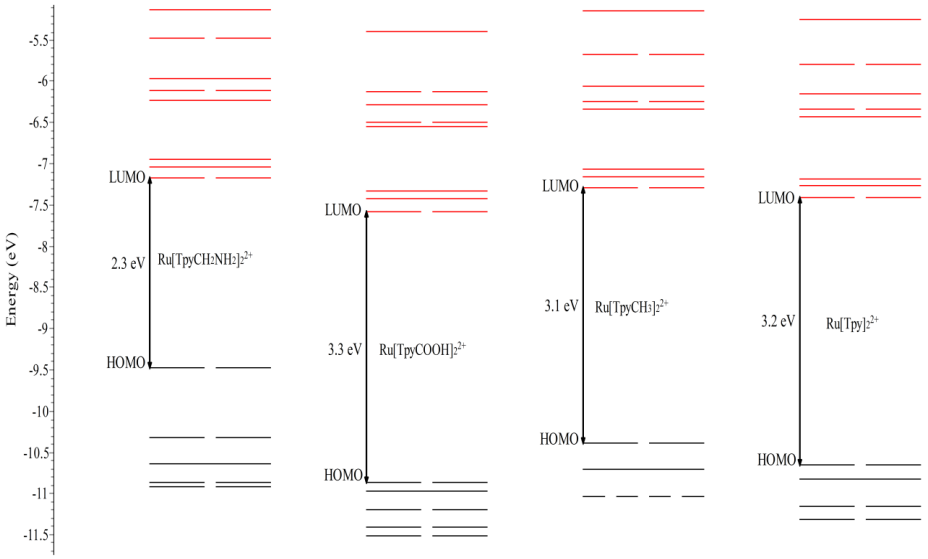

Figure 2. Molecular orbital diagram showing HOMO-LUMO gap calculated at B3LYP/LanL2DZ level of theory.

Table 2. Energies of $[Ru(TpyCH_2NH_2)_2]^{2+}$

Functional/basis sets	Energy (Hartrees)		HOMO-LUMO (eV)
	HOMO	LUMO	
B3LYP/LanL2DZ	-0.34283	-0.26446	2.1
B3LYP/3-21G	-0.33719	-0.25854	2.1
X3LYP/ LanL2DZ	-0.34507	-0.26089	2.3
X3LYP/3-21G	-0.33941	-0.25457	2.3
B3PW91/LanL2DZ	-0.34448	-0.26685	2.1
B3PW91/3-21G	-0.33996	-0.26326	2.1

Small HOMO-LUMO energy gaps of Ru complexes have been frequently reported. For example, HOMO-LUMO energy gaps of 2.5-2.7eV have been recently estimated by cyclic voltametry of a Ru complex with similar bipyridine (Bpy) and terpyridine ligands (10-13), and the HOMO-LUMO energy gaps of $[Ru(Bpy)_3]^{2+}$ and $[Ru(Tpy)_2]^2$ were predicted to be 2.64 and 2.51 eV, respectively [10-13].

The HOMO-LUMO gap was determined by spectroscopic methods. From **Table 3**, the HOMO-LUMO energy gap of $[Ru(TpyCH_2NH_2)_2]^{2+}$ and $[Ru(TpyCH_3)_2]^{2+}$ were close to their energy at zero vibration energy level (E_{0-0}): 1.91 and 3.72 eV, respectively. These values are comparable to the predicted HOMO-LUMO gaps. However, the HOMO-LUMO gap of $[Ru(Tpy)_2]^{2+}$ of 2.13 eV was lower than the predicted value of 3.2 eV. The cyclic voltammogram experiment was carried out in a MeCN solution of 0.04 mg/ml $[Ru(TpyCH_2NH_2)_2]^{2+}$ with scanning rate of 100 mV/s **(Figure 3)**. The reduction and oxidation onset potentials are obtained as $E_{onset,\ red}$ (-1.00 V/SCE) and $E_{onset,\ ox}$ (+1.33 V/SCE), respectively. The HOMO-LUMO energy gap can be calculated by substituting the measured onset potential. We can calculate that the HOMO-LUMO energy gap of $[Ru(TpyCH_2NH_2)_2]^{2+}$ is 2.3 eV according to the relationship of Hamiltonian calculation and electrochemical method [8]. This value is lower than the reported 2.51 eV $[Ru(Tpy)_2]^{2+}$ **(Table 3)**.

Table 3. The electronic properties of $[RuTpyCH_2NH_2)_2]^{2+}$, $[Ru(TpyCH_3)_2]^{2+}$ and $[Ru(Tpy)_2]^{2+}$.

Photo physical Properties	$[Ru(TpyCH_2NH_2)_2]^{2+}$ [a]	$[Ru(TpyCH_3)_2]^{2+}$ [b]	$[Ru(Tpy)_2]^{2+}$ [b]
UV-VIS Absorption λmax/nm (10^4ε/dm^{3}mol^{-1} cm^{-1})	252(5.07);276 (5.26) (π-π*)	283(5.69) (π-π*)	271(5.59) (π-π*)
	314 (2.67) (IL, n-π*)	307 (6.65) (IL, n-π*)	309(7.02) (IL, n-π*)
	493 (0.95) (ILCT, n-dπ*)	488 (2.64), 490(2.89)[a] (^{1}MLCT ,dπ-π)	476(1.77) 476 (1.04)[a] (^{1}MLCT,dπ-π*)
Emission λmax (nm)	687	650 (^{3}MLCT)	629[a](^{3}MLCT)
E_{0-0} (eV)	1.91	3.72	2.13
HOMO-LUMO gap (eV)	2.3 2.3[c]	3.1[c]	2.51 3.2[c]

[a]The electronic spectra $[Ru(TpyCH_2NH_2)_2]^{2+}$ and $[Ru(Tpy)_2]^{2+}$ are measured in acetonitrile, tTpy = 4′-tolyl-2, 2′: 6′, 2″ terpyridine. The fluorescence excitation wavelength is (λex= 290 nm) in DSMO solvent at 298 K. [b] Data reported in Ref. 37-42, ethanol was used as a solvent. [c] Calculations performed at B3LYP/LANL2DZ level of theory.

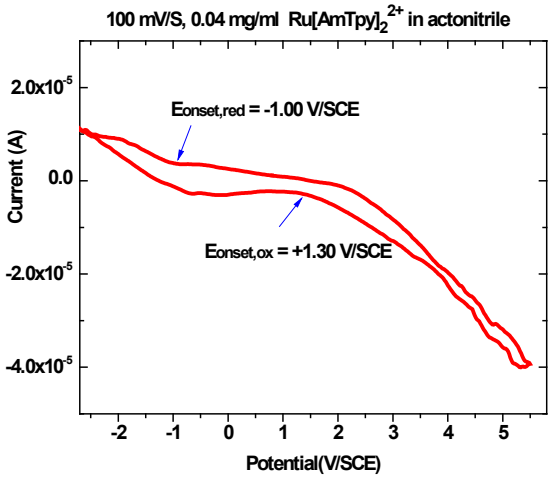

Figure 3. The cyclic voltammogram of $[Ru(TpyCH_2NH_2)_2]^{2+}$ in acetonitrile Working Electrode: Solid Electrode Working Electrode Area: 1.000 cm² Reference Electrode: Ag, AgCl / NaCl (sat'd) (0.194 V).

Electronic Spectra of Ru Complexes

Figure 4a shows the UV-Vis spectra of $[Ru(TpyCH_2NH_2)_2]^{2+}$, $[Ru(TpyCOOH)_2]^{2+}$, and $[RuTpyCH_3)_2]^{2+}$ complexes. As expected, the spectra of these complexes are similar. Two intense absorption peaks dominate the spectra while a weak peak is observed at the low energy side of the spectrum. There are two major peaks in the spectra. One peak at 200-400 nm region has been traditionally assigned to ligand centered (LC) π-π* transitions of the terpyridine pyridine aromatic rings [36]. Another major peak is at 400-600 nm that is traditionally used for metal-ligand interaction in the excited states. In these spectra, there is a slight blue shift of peaks from $[RuTpyCH_3)_2]^{2+}$, $[Ru(TpyCH_2NH_2)_2]^{2+}$ to $[Ru(TpyCOOH)_2]^{2+}$ in the 200-400 nm region Such transition blueshifts are due to differences in functional group electronic effect of substituted terpyridine ligands [36]. The substituent groups cause redshift and intensity variance for peaks in 400-650 nm region: $[RuTpyCH_3)_2]^{2+}$>$[Ru(TpyCH_2NH_2)_2]^{2+}$>$[Ru(TpyCOOH)_2]^{2+}$. **(Figure 4a)** The solutions of these ruthenium complexes have colors that range from red to pink **(Figure 4b)**.

The fluorescence spectrum of $[Ru(TpyCH_2NH_2)_2]^{2+}$ show two major emission peaks at 344-364 nm and 687-709 nm when excited at 290 nm laser wavelength **(Figure 4c)**. Based on the Stoke's shift, the energy of zero vibration energy level (E_{0-0}) of $[Ru(TpyCH_2NH_2)_2]^{2+}$ was measured by the curve crossing point (328 nm) of the absorption and emission spectra when a laser exited wavelength is 290 nm.

To assign electronic transitions to the observed UV-Vis peaks, TD-DFT calculations of the complexes were performed **(Table 4 a-c)**. TDDFT method was used to study and estimate the excitation properties of ruthenium complex spectra. Figure 4 shows TD-DFT predicted spectra of $[Ru(TpyCH_3)_2]^{2+}$, $[Ru(TpyCH_2NH_2)_2]^{2+}$ and $[Ru(TpyCOOH)_2]^{2+}$. The general patterns of the UV-Vis spectra **(Figure 4a)** of these complexes are comparable to the TD-DFT spectra **(Figure 5)**. As results, the predicted excitations were used to better understand the interpretation of the spectra. **Table 3** shows the peak assignments.

The UV-Vis spectrum of $[Ru(TpyCH_2NH_2)_2]^{2+}$ has a major peak at 493 nm. This low energy peak is important because it is typically assigned for molecular orbitals that may involve the d-orbitals of Ru. Using TD-DFT data **(Table 2)**, this peak correlates with two predicted strong singlet excited states (427 nm with f = 0.2267 and 493 nm with f = 0.3799). These states correspond to the following transitions: HOMO → LUMO (45%), HOMO-1 → LUMO+1 (45%), and HOMO-2 → LUMO+2 (94%). Note that both the HOMO and HOMO-1 are all ligand orbitals while LUMO and LUMO+1 have a minor 8% contribution of Ru orbitals **(Table 3)**; this molecular orbital composition make both HOMO → LUMO (45%) and HOMO-1 → LUMO+1 (45%) ILCT transition **(Table 4 a-c)**. Other minor contributions to the UV-Vis peak at 493 nm in the $[Ru(TpyCH_2NH_2)_2]^{2+}$ spectrum are HOMO-2 → LUMO (89%) and HOMO-2 → LUMO+1 (90%) transitions **(Table 4 a-c)**. Since HOMO-2 has 34% Ru contribution, these transitions have some minor MLCT characteristic. Therefore, the peak at 493 nm in the $[Ru(TpyCH_2NH_2)_2]^{2+}$ spectrum is assigned as inner-ligand charge

transfer (ILCT) with minor contribution of MLCT. The proposed inner-ligand charge transfer is a special case of all-organic charge transfer (OCT) states described as non-hydrocarbon π electron system [1,2]. This ILCT transition at 493 nm, which, if this is really relative to the HOMO-LUMO transition, should be different in terms of energy when compared to the corresponding feature in the simple $[Ru(Tpy)_2]^{2+}$ complex. In particular, the calculations predict that there is a decrease in the HOMO-LUMO gap in $[Ru(TpyCH_2NH_2)_2]^{2+}$ as compared to $[Ru(Tpy)_2]^{2+}$, the corresponding band at 493 nm in $[Ru(TpyCH_2NH_2)_2]^{2+}$ shifted to lower energy than that of reported $[Ru(TpyCH_3)_2]^{2+}$, MLCT at 490 nm, and $[Ru(Tpy)_2]^{2+}$, MLCT at 476 nm in acetonitrile [1,2,37-42] **(Table 5)**.

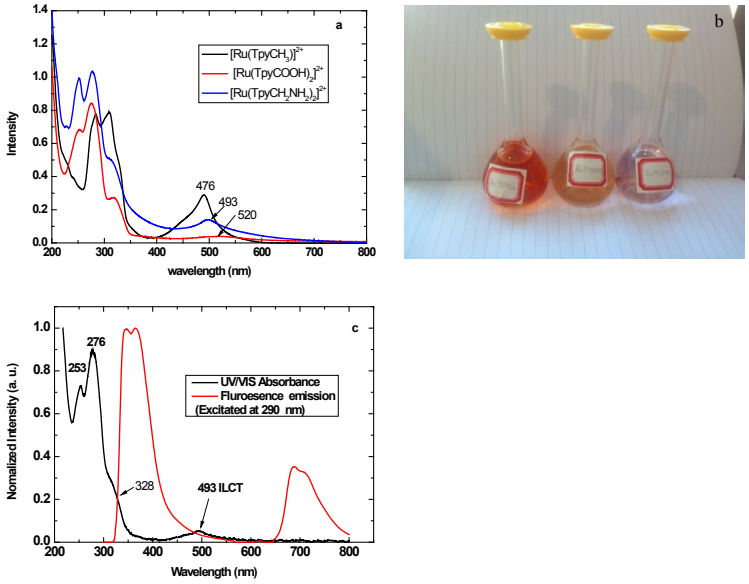

Figure 4. a) UV-Vis spectra of ruthenium terpyridine complexes; b) The samples of ruthenium terpyridine complexes in MeCN: from left to right are 0.01mg/ml $[Ru(TpyCH_3)_2]^{2+}$,0.02 mg/ml $[Ru(TpyCH_2NH_2)_2]^{2+}$and $[Ru(TpyCOOH)_2]^{2+}$ respectively c) The normalized electronic spectra of $[Ru(TpyCH_2NH_2)_2]^{2+}$.

Table 4 a. Assignments of transitions (High than 10% contribution) by TD-DFT at B3LYP/LANL2DZ level of theory in the UV-Vis spectrum of $[Ru(TpyCH_2NH_2)_2]^{2+}$, $[Ru(TpyCOOH)_2]^{2+}$ and $[Ru(TpyCH_3)_2]^{2+}$

TD-DFT Predicted	Transitions (contribution)	f(Osc. Strength)	$10^4\varepsilon/dm^3mol^{-1}\ cm^{-1}$
291.44	HOMO-1→LUMO+8 (18%) HOMO-1→LUMO +9 (25%) HOMO→ LUMO+8 (26%) HOMO→ LUMO+9 (18%)	0.4799	5.07
298.80	HOMO -10→LUMO (15%) HOMO-10→ LUMO+1 (54%) HOMO -6→ LUMO+3 (16%)	0.2402	
298.82	HOMO-10→LUMO (54%), HOMO-10→ LUMO +1 (16%) HOMO-5→ LUMO+3 (15%)	0.2428	
302.96	HOMO -9→LUMO (84%)	0.2013	5.26
302.94	HOMO -9→LUMO+1 (84%)	0.2012	
317.53	HOMO -6→ LUMO+2 (54%) HOMO -6→ LUMO +3 (25%)	0.0243	2.67
317.58	HOMO -5→ LUMO +2 (54%) HOMO-5→ LUMO +3 (25%	0.0241	
325.89	HOMO -6→LUMO (24%) HOMO-6→ LUMO+1 (14%) HOMO -5→LUMO (14%) HOMO-5→ LUMO +1 (23%) HOMO -2→ LUMO+4 (23%)	0.0931	
330.42	HOMO -1→ LUMO+5 (27%) HOMO-1→ LUMO +6 (19%) HOMO→ LUMO+5 (20%) HOMO→ LUMO+6 (27%)	0.1948	
427.62	HOMO-2→LUMO+2 (94%)	0.2267	0.95
472.34	HOMO-1→LUMO+1 (45%) HOMO→LUMO (45%)	0.3799	
496.87	HOMO-2→LUMO (89%)	0.0141	
496.83	HOMO-2→LUMO+1 (90%)	0.0144	

e-ISSN:2319-9849
p-ISSN:2322-00

B

$[Ru(TpyCH_3)_2]^{2+}$				
λmax/nm	TD-DFT Predicted	Transitions (contribution)	f(Osc. Strength)	$10^4\varepsilon/dm^3mol^{-1}\ cm^{-1}$
284	277.58	HOMO-7→LUMO+3 (58%) HOMO-6→LUMO+2 (25%) HOMO-5→LUMO+3 (13%)	0.264	7.72
	278.55	HOMO-8→LUMO+2 (38%) HOMO-5→LUMO+3 (42%)	0.6734	
	295.76	HOMO-6→LUMO+2 (50%) HOMO-5→LUMO+3 (19%)	0.2111	7.87
310	297.65	HOMO-6→LUMO+2 (15%) HOMO-1→LUMO+9 (33%) HOMO→LUMO+8 (33%)	0.2498	
	304.15	HOMO-8→LUMO (45%) HOMO-8→LUMO+1 (24%)	0.3194	
	304.15	HOMO-8→LUMO (24%), HOMO-8→LUMO+1 (45%)	0.3195	
	309.72	HOMO-7→LUMO+1 (14%) HOMO-5→LUMO (10%) HOMO-5→LUMO+1 (46%)	0.1280	
	309.72	HOMO-7→LUMO (14%) HOMO-5→LUMO (46%) HOMO-5→LUMO+1 (10%)	0.1272	
329	330.28	HOMO-4→LUMO (18%) HOMO-4→LUMO+1 (11%) HOMO-3→LUMO (11%) HOMO-3→LUMO+1 (18%) HOMO-2→LUMO+4 (40%)	0.0561	4.73
	333.88	HOMO-1→LUMO+5(43%) HOMO→LUMO+6 (43%)	0.1876	
	333.88	HOMO-1→LUMO+5 (27%) HOMO-1→LUMO+6 (19%) HOMO→LUMO+5 (20%) HOMO→LUMO+6 (27%)	0.1948	
	338.54	HOMO-4→LUMO (13%) HOMO-3→LUMO+1 (13%) HOMO-2→LUMO+4 (56%)	0.3830	
490	432.98	HOMO-2→LUMO+2 (93%)	0.2438	2.89
	476.51	HOMO-1→LUMO (30%) HOMO-1→LUMO+1 (16%) HOMO→LUMO (16%) HOMO→LUMO+1 (30%)	0.3903	

c.

$[Ru(TpyCOOH)_2]^{2+}$				
λmax/nm	**TD-DFT Predicted**	**Transitions (contribution)**	**f(Osc. Strength)**	**$10^4\varepsilon/dm^3mol^{-1}\ cm^{-1}$**
252	278.53	HOMO-8→LUMO+3 (23%) HOMO-7→LUMO+2 (44%) HOMO-4→LUMO+2 (10%) HOMO-3→LUMO+3 (17%)	0.1637	3.40
276	280.49	HOMO-8→LUMO+3 (11%) HOMO-7→LUMO+2 (21%) HOMO-4→LUMO+2 (22%) HOMO-3→LUMO+3 (39%)	0.4196	4.20
	299.25	HOMO-8→LUMO (32%) HOMO-8→LUMO+1 (14%) HOMO-7→LUMO (14%) HOMO-7→LUMO+1 (33%)	0.0719	

319	308.65	HOMO-4→LUMO+1 (31%) HOMO→LUMO+7(18%) HOMO→LUMO+8 (33%)	0.3029	1.36
	308.65	HOMO-4→LUMO (31%) HOMO→LUMO+7 (33%) HOMO→LUMO+8 (18%)	0.3029	
	324.15	HOMO-4→LUMO (10%) HOMO-3→LUMO (32%) HOMO-1→LUMO+14 (11%) HOMO→LUMO+7 (16%)	0.0645	
	324.15	HOMO-4→LUMO+1 (10%) HOMO-3→LUMO+1 (32%) HOMO-2→LUMO+14 (11%) HOMO→LUMO+8 (16%)	0.0645	
	331.27	HOMO→LUMO+6 (94%)	0.0681	
	348.37	HOMO-2→LUMO+4 (44%) HOMO-1→LUMO+5 (44%)	0.4092	
522	432.01	HOMO→LUMO+2 (93%)	0.2689	0.196
	434.93	HOMO-1→LUMO+2 (89%)	0.0219	
		HOMO-2→LUMO+2 (89%)	0.0218	
	476.02	HOMO-2→LUMO (34%) HOMO-2→LUMO+1 (11%) HOM O-1→LUMO (11%) HOMO-1→LUMO+1 (34%)	0.4473	
	516.68	HOMO→LUMO+1 (89%)	0.0103	
	516.71	HOMO→LUMO (91%)	0.0104	

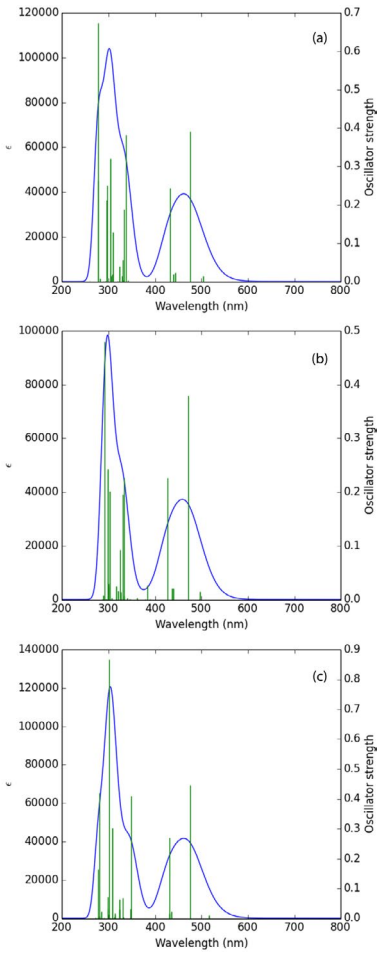

Figure 5. The TD-DFT predicted UV-Vis spectra of Ruthenium terpyridine complexes. a) $[Ru(TpyCH_3)_2]^{2+}$, b)

On the other hand, $[Ru(TpyCH_3)_2]^{2+}$, the experimental band at 490 nm is assigned as MLCT. Two singlet states such as 433 nm with f = 0.2438 and 477 nm with f = 0.3903 are mainly characterized by the transition of HOMO-2 → LUMO+2(93%) or degenerated HOMO → LUMO+1 (30%) and HOMO-1 → LUMO (30%) mixed with minor contributions of degenerated HOMO → LUMO (16%) and HOMO-1 → LUMO+1 (16%). Those transition MOs have major Ru composition. For instance, HOMO/HOMO-1 has 36% and HOMO-2 has 78% Ru composition for excited states. Thus, the 490 nm band has a strong Ru metal contribution.

Therefore, the peak at 490 nm is assigned as MLCT. Based on the similar assignment method and experimental data, the absorption bands of $[Ru(TpyCOOH)_2]^{2+}$ at 520 nm and $[Ru(Tpy)_2]^{2+}$ at 476 nm are attributed to MLCT. Similar assignments of UV-Vis peaks have been previously described [34, 43], that have significant contribution by Ru d-orbitals.

Table 5. Assignments of transitions (High than 10% contribution) by TD-DFT at B3LYP/LANL2DZ level of theory in the UV-Vis spectrum of $[Ru(TpyCH_2NH_2)_2]^{2+}$, $[Ru(TpyCOOH)_2]^{2+}$ and $[Ru(TpyCH_3)_2]^{2+}$ in 400-600 nm region.

$[Ru(TpyCH_2NH_2)_2]^{2+}$				
λmax/nm	**TD-DFT Predicted**	**Transitions (contribution)**	**f(Osc. Strength)**	**$10^4\varepsilon$/dm^{3}mol^{-1} cm^{-1}**
493	427.62	HOMO-2→LUMO+2 (94%)	0.2267	0.95
	472.34	HOMO-1→LUMO+1 (45%) HOMO→LUMO (45%)	0.3799	
	496.87	HOMO-2→LUMO (89%)	0.0141	
	496.83	HOMO-2→LUMO+1 (90%)	0.0144	
$[Ru(TpyCOOH)_2]^{2+}$				
λmax/nm	**TD-DFT Predicted**	**Transitions (contribution)**	**f(Osc. Strength)**	**$10^4\varepsilon$/dm^{3}mol^{-1} cm^{-1}**
522	432.01	HOMO→LUMO+2 (93%)	0.2689	0.196
	434.93	HOMO-1→LUMO+2 (89%)	0.0219	
		HOMO-2→LUMO+2 (89%)	0.0218	
	476.02	HOMO-2→LUMO (34%) HOMO-2→LUMO+1 (11%) HOM O-1→LUMO (11%) HOMO-1→LUMO+1 (34%)	0.4473	
	516.68	HOMO→LUMO+1 (89%)	0.0103	
	516.71	HOMO→LUMO (91%)	0.0104	
$[Ru(TpyCH_3)_2]^{2+}$				
λmax/nm	**TD-DFT Predicted**	**Transitions (contribution)**	**f(Osc.Strength)**	**$10^4\varepsilon$/dm^{3}mol^{-1} cm^{-1}**
490	432.98	HOMO-2→LUMO+2 (93%)	0.2438	2.89
	476.51	HOMO-1→LUMO (30%) HOMO-1→LUMO+1 (16%) HOMO→LUMO (16%) HOMO→LUMO+1 (30%)	0.3903	

Cellular Uptake and Proliferative Response of Human Cancer Cells to Ruthenium Complexes

Ruthenium complexes characterized by their uptake and luminescence stability in cells have considered as therapeutic or diagnostic agents [9,44-45]. The present study examined the cellular uptake and proliferative response to Ru (II) terpyridine complexes with carboxylic (R1= $[Ru(TpyCOOH)_2]^{2+}$) and amino (R2= $[Ru(TpyCH_2NH_2)_2]^{2+}$) groups in 647V human bladder cancer cell line, incubated with different concentration of the Ru (II) terpyridine complexes. Results from the cellular uptake assay in this study were similar to the reported observation of Hela cells exposed to Ru (II) dipyridophenazine complexes [2,9,44-45]. The amino complex group exhibited biologic activity as measured by dose-dependent decrease in rate of proliferation when cells are incubated with the compound for 24 hours.

The ruthenium complex is readily transferred into the cellular interior rather than being associated solely within the membrane surface. Cellular uptake of ruthenium complexes by cancer cell line shows the apparent cytoplasmic location of $[Ru(TpyCH_2NH_2)_2]^{2+}$ monitored at 488 nm by live imaging with fluorescence microscope, likely associated with the mitochondria and endoplasmic reticulum **(Figure 6a-c)**, when incubated with 10 µm Ru complex. The fluorescence emission of $[Ru(TpyCH_2NH_2)_2]^{2+}$ remain evident in cells after 24 hours incubation period. On the other hand, the fluorescence imaging of $[Ru(TpyCOOH)_2]^{2+}$ in cells is too weak to be detectable and cellular uptake location of $[Ru(TpyCOOH)_2]^{2+}$ is diffused in cells **(Figure 6d-f)**. $[Ru(TpyCH_2NH_2)_2]^{2+}$ had better cellular uptake effect than $[Ru(TpyCOOH)_2]^{2+}$. Uptake of $[Ru(TpyCH_2NH_2)_2]^{2+}$ appeared more stable because the fluorescence of the complex is detectable after 24hours exposure. The differences in uptake of $[Ru(TpyCOOH)_2]^{2+}$ and $[Ru(TpyCH_2NH_2)_2]^{2+}$ by the bladder cell line is due to lipophilicity and hydrophobicity of those ruthenium compounds, which is close relative to cellular uptake and bimolecular binding. Our results showed that $[Ru(TpyCOOH)_2]^{2+}$ with low lipophilicity are diffused in the cells and the lipophilicity derivative of $[Ru(TpyCH_2NH_2)_2]^{2+}$ localized to the cell cytoplasm. Our results showed that the ruthenium complex with the basic amine group has higher cellular uptake, which therefore makes it more bio-available to mediate anti-proliferation effects.

The amino groups of $[Ru(TpyCH_2NH_2)_2]^{2+}$ can assist in enhancing the cytoplasmic location due to hydrophilic interactions through hydrogen bond formation with amino acid residues or sugars of intracellular tissue in the cytoplasm. The effect on cellular proliferation represents a new observation with a Ru complex. The cytotoxic effect of both requested treatment at high concentration of Ru terpyridine complexes (about 1µM to 10 µM). The proliferation response of bladder 647V cell line depicts that $[Ru(TpyCH_2NH_2)_2]^{2+}$ is only cytotoxic at the highest 50 um dose exposure **(Figure 7)**. Biological activity based on the proliferation

assay, indicate a dose-dependent decrease in the proliferation of 647V cells exposed to $[Ru(TpyCH_2NH_2)_2]^{2+}$, but $[Ru(TpyCOOH)_2]^{2+}$ does not mediate a measurable biological effect on cells and does not have apparent cytotoxic effect as determined by the similar rate of proliferation. Compared to $[Ru(TpyCOOH)_2]^{2+}$, **Figure 6** show that $[Ru(TpyCH_2NH_2)_2]^{2+}$ decreased the proliferation capacity of cells in a dose dependent manner over a 24 hour incubation period. As the results, $[Ru(TpyCH_2NH_2)_2]^{2+}$ is stabilized luminescence in cytoplasmic location and low cytotoxic effect for diagnostic cancer cell line with obvious luminescence. The effect on cellular proliferation suggests that the Ru terpyridine complex may be considered for biomedical applications as a potential bio-imaging agent.

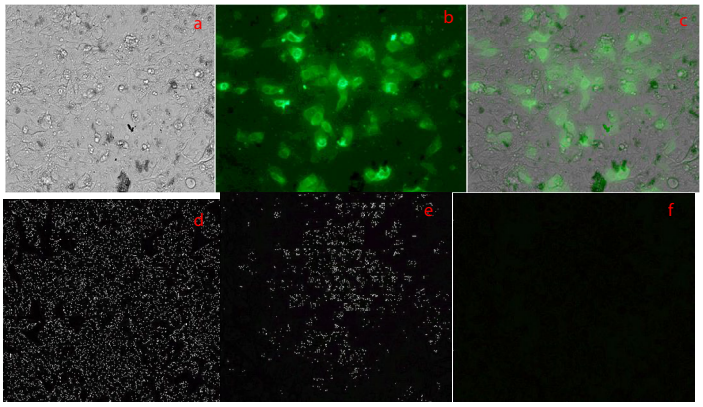

Figure 6. Fluorescent Image of $[Ru(TpyCH_2NH_2)_2]^{2+}$; $[Ru(TpyCOOH)_2]^{2+}$ complex accumulation in 647V cells, cells were incubated with 10uM Ru terpyridine complex for 1 hour at 37°C, 5% CO_2. a) Microscopic image under white light b) Fluorescent microscopic image monitored at 488 nm wavelengths. c)The overlay image of a) and b); $[Ru(TpyCOOH)_2]^{2+}$ complex: d) Microscopic image under white light e) Fluorescent microscopic image monitored at 488 nm wavelengths. f) The overlay image of d) and e).

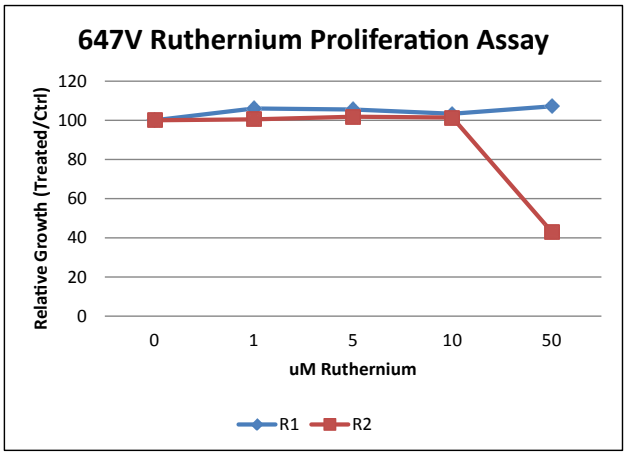

Figure 7. The 647 relative proliferation rate by control untreated cells and cells treated with R1=$[Ru(TpyCOOH)_2]^{2+}$, R2=$[Ru(TpyCH_2NH_2)_2]^{2+}$.

CONCLUSIONS

The results of this study demonstrate the effect of introducing a CH_2NH_2 group as part of terpyridine in $[Ru(TpyCH_2NH_2)_2]^{2+}$. $[Ru(TpyCH_2NH_2)_2]^{2+}$ has the lowest HOMO-LUMO gap of 2.3 eV among the Ruthenium terpyridine complexes examined. The HOMO–LUMO gaps of DFT calculation (2.3 eV) is consistent with the results measured from its electronic spectroscopy (1.91 eV) and electrochemical experimental result (2.3 eV). Results suggest that a long-range ligand substituent effect on the Ru metal center leads to an all-ligand HOMO composition. The $[Ru(TpyCH_2NH_2)_2]^{2+}$ HOMO composition is altered by the substituted amino groups of terpyridine ligand. All-ligand composited HOMO suggest that the traditional metal-to-ligand charge transfer is no longer possible in $[Ru(TpyCH_2NH_2)_2]^{2+}$. Molecular orbital compositions and TD-DFT analysis indicated that the peak at 493 nm in the UV-Vis spectrum of $[Ru(TpyCH_2NH_2)_2]^{2+}$ is dominated by inter ligand charge transfer from orbitals involving the amino group. Moreover, lowering the HOMO-LUMO gap of the ruthenium complex is associated with the introduction of amino groups. This confirmed using metal-remote functional group is a viable strategy of model new materials. The cellular uptake and apparent fluorescence properties of $[Ru(TpyCH_2NH_2)_2]^{2+}$ in 647V bladder cancer cells could be found potential application for bioimaging.

SUPPLEMENTARY MATERIALS

The characterization of $[Ru(TpyCH_2NH_2)_2](BF_4)_2$ complex is regarded in supporting materials. The TD-DFT predicted UV-Vis spectrum data of $[Ru(TpyCH_2NH_2)_2]^{2+}$, $[Ru(TpyCOOH)_2]^{2+}$ and $[Ru(TpyCH_3)_2]^{2+}$ complexes are also provided in detail.

ACKNOWLEDGMENTS

The authors thank the National Science Foundation (NSF/CFNM/ CREST program, grant Award # HRD-11137751) for financial support for this research

REFERENCES

1. De Silva P, Gunaratne HQN, Gunnlaugsson T, Huxley AJM, McCoy CP, et al. Signaling recognition events with fluorescent sensors and switches. Chem Rev. 1997; 97:1515-1566.
2. Sauvage JP, Collin JP, Chambron JC, Guillerez S, Coudret C, et al. Ruthenium(II) and Osmium(II) Bis(terpyridine) Complexes in Covalently-Linked Multicomponent Systems: Synthesis, Electrochemical Behavior, Absorption Spectra, and Photochemical and Photophysical Properties. Chem Rev. 1994; 94:993–1019.
3. Li H, Wu J, Jeilani YA, Ingram CW, Harruna II. Modification of multiwall carbon nanotubes with ruthenium(II) terpyridine complex. J Nanopart Res. 2012; 14:847.
4. Li H. Wu J, Ingram CW, Harruna II. Functionalization of multi-walled carbon nanotubes with bis(2,2':6',2"-terpyridine) ruthenium(II)-connected diblock polymer. J Nanosci Nanotech. 2012; 12:3739-3750.
5. Reuven DG, Li H, Harruna II, Wang XQ. Self-assembly of metallopolymer guided by graphene nanoribbons J Mater Chem. 2012; 22:15689-15694.
6. Nazeeruddin MK, Kay A, Rodicio I, Humphry-Baker R, Mueller E, et al. Conversion of light to electricity by cis-X2bis(2,2'-bipyridyl-4,4'-dicarboxylate)ruthenium(II) charge-transfer sensitizers (X = Cl-, Br-, I-, CN-, and SCN-) on nanocrystalline titanium dioxide electrodes. J Am Chem Soc. 1993; 115:6382-6390.
7. Coury JE, Anderson JR, McFail-Isom L, Williams LD, Bottomley LA. Scanning force microscopy of small ligand−nucleic acid complexes: tris(o-phenanthroline)ruthenium(II) as a test for a new assay. J Am Chem Soc. 1997; 119:3792-3796.
8. Lee N, Shin H, Kim Y, Kim C, Suh S. HOMO-LUMO energy gap analysis of alkyl viologen with a positively charged aromatic ring. Rev Roum Chim. 2010; 55:627-632.
9. Puckett CA, Barton JK. Methods to explore cellular uptake of ruthenium complexes. J Am Chem Soc. 2007; 129:46-47.
10. Mete E. Uner D, Çakmak M, Gulseren O, Ellialtolu S. Novel synthesis of pyrrolidinones by cobalt carbonyl catalyzed carbonylation of azetidines. A new ring-expansion-carbonylation reaction of 2-vinylazetidines to tetrahydroazepinones. J Phys Chem. 2007; 111:7539-7543.
11. Cances MT, Mennucci B, Tomasi J. A new integral equation formalism for the polarizable continuum model: Theoretical background and applications to isotropic and anisotropic dielectrics. J Chem Phys. 1997; 107:3032-3041.
12. Tomasi J, Persico M, Molecular interactions in solution: An overview of methods based on continuous distributions of the solvent. Chem Rev. 1994; 94:2027-2094.
13. Cossi M, Barone V, Mennucci B, Tomasi J. Ab initio study of ionic solutions by a polarizable continuum dielectric model. Chem Phys Lett. 1998; 286:253-260.
14. Ma R, Guo P, Yang L, Guo L, Zhang X, et al. Theoretical screening of −NH2-, −OH-, −CH3-, −F-, and −SH-substituted porphyrins as sensitizer candidates for dye-sensitized solar cells. J Phys Chem. 2010; 114:1973-1979.
15. Mennucci B, Tomasi J. Continuum solvation models: A new approach to the problem of solute's charge distribution and cavity boundaries. J Chem Phys. 1997; 106:5151-5158.
16. Lutterman DA, Chouai A, Liu Y, Sun Y, Stewart CD, et al. Intercalation is not required for DNA light-switch behavior. J Am Chem Soc. 2008; 130:1163-1170.
17. Reed AE, Weinstock RB, Weinhold F. Natural population analysis. J Chem Phys. 1985; 83:735-746.
18. Frisch MJ, Trucks GW, Schlegel HB, Scuseria GE, Robb MA et al. Gaussian 09, Gaussian, Inc., Wallingford CT.
19. Becke D. Density-functional exchange-energy approximation with correct asymptotic behavior. Phys Rev. 1988; 38:3098-3100.
20. Lee C, Yang W, Parr RG. Development of the Colle-Salvetti correlation-energy formula into a functional of the electron density. Phys Rev. 1988; 37:785-789.
21. Xu X, Goddard WA. The X3LYP extended density functional for accurate descriptions of nonbond interactions, spin states, and thermochemical properties. Proc Natl Acad Sci. 2004; 101:2673-2677.
22. Baker J, Pulay P. Assessment of the Handy–Cohen optimized exchange density functional for organic reactions. J Chem Phys. 2002; 117:1441-1449.
23. Perdew JP, Chevary JA, Vosko SH, Jackson KA, Pederson MR. Atoms, molecules, solids, and surfaces: Applications of the

generalized gradient approximation for exchange and correlation. Phys Rev. 1992; 46:6671-6687.

24. Hay PJ, Wadt WR. Ab initio effective core potentials for molecular calculations. Potentials for the transition metal atoms Sc to Hg. J Chem Phys. 1985; 82:270-284.

25. Wadt WR, Hay PJ. Ab initio effective core potentials for molecular calculations. Potentials for main group elements Na to Bi. J Chem Phys. 1985; 82:284-298.

26. Hay PJ, Wadt WR. Ab initio effective core potentials for molecular calculations. Potentials for K to Au including the outermost core orbitals. J Chem Phys. 1985; 82:299-310.

27. Dobbs KD, Hehre WJ. Molecular orbital theory of the properties of inorganic and organometallic compounds 4. Extended basis sets for third-and fourth-row, main-group elements. J Comp Chem. 1986; 7:359-378.

28. GaussView 3.0 User's Reference. Gaussian, Inc.: Wallingford, CT, USA.

29. Tang BF, Yu P, Li L, Tong X, Duan T, et al. A near-infrared neutral pH fluorescent probe for monitoring minor pH changes: imaging in living hepg2 and hl-7702 cells. J Am Chem Soc. 2009; 131:3016-3023.

30. Kelch S, Rehahn M. Synthesis and properties in solution of rodlike, 2, 2':6',2''-terpyridine-based ruthenium(II) coordination polymers. Macromolecules. 1999; 32:5818-5828.

31. Collin JP, Harriman A, Heitz V, Odobel F, Sauvage JP. Photoinduced electron- and energy-transfer processes occurring within porphyrin-metal-bisterpyridyl conjugates. J Am Chem Soc. 1994; 116:5679-5690.

32. Stublla A, Potvin PG. Ruthenium(II) complexes of carboxylated terpyridines and dipyrazinylpyridines. Eur J Inorg Chem. 2010; 19:3040-3050.

33. Ciofini I, Daul CA, Adamo C. Phototriggered Linkage Isomerization in ruthenium−dimethylsulfoxyde complexes:Insights from theory. J Phys Chem. 2003; 107:11182-11190.

34. Gopakumar TG, Meiss J, Pouladsaz D, Hietschold M. HOMO−LUMO Gap Shrinking Reveals Tip-Induced Polarization of Molecules in Ultrathin Layers: Tip−Sample Distance-Dependent Scanning Tunneling Spectroscopy on d8 (Ni, Pd, and Pt) Phthalocyanines. J Phys Chem. 2008; 112:2529-2537.

35. Lundqvist MJ, Nilsing M, Lunell S, Åkermark B, Persson P. Spacer and anchor effects on the electronic coupling in ruthenium-bis-terpyridine dye-sensitized TiO2 nanocrystals studied by DFT. J Phys Chem. 2006; 110:20513-20525.

36. Yao CJ, Yao J, Zhong YW. Electronic communication between two amine redox centers bridged by a bis(terpyridine) ruthenium(II) complex Inorg Chem. 2011; 50:6847-6849.

37. Amouyal E, Mouallem-Bahout M. Photophysical study of tolylterpyridine complexes. Intramolecular electron transfer in an osmium (II) dyad. J Chem Soc Dalton Trans. 1992; 509-513.

38. Hewitt JT, Vallet DJ, Damarauer NH. Dynamics of the ^{3}MLCT in Ru terpyridyl complexes probed by ultrafast spectroscopy: Evidence of excited-state equilibration and interligand electron transfer. J Phys Chem. 2012; 116:11536-11547.

39. Jakubikova EE, Chen W, Dattelbaum DW, Rein FN, Rocha RC. Electronic structure and spectroscopy of $[Ru(Tpy)_2]^{2+}$, $[Ru(Tpy)(bpy)(H_2O)]^{2+}$, and $[Ru(Tpy)(bpy)(Cl)]^{+}$. Inorg Chem. 2009; 48:10720-10725.

40. Beley M, Collins JP, Sauvage JP, Sugihara H, Heisel F, et al. Photophysical and photochemical properties of ruthenium and osmium complexes with substituted terpyridines. J Chem Soc Dalton Trans. 1991; 3157-3159.

41. Maestri M, Armaroli N, Balzani V, Constable EC, Cargill Thompsonlb AMW. Complexes of the ruthenium(II)-2,2':6',2''-terpyridine family, Effect of electron-accepting and -donating substituents on the photophysical and electrochemical propertie. Inorg Chem. 1995; 34:2579–2767.

42. Brown DG, Sanguantrakun N, Schulze B, Schubert US. Bis(tridentate) ruthenium–terpyridine complexes featuring microsecond excited-State lifetimes. J Am Chem Soc. 2012; 134:12354-12357.

43. Ding H, Wang X, Song L, Chen J, Yu J. Aryl-modified ruthenium bis(terpyridine) complexes: Quantum yield of 1O2 generation and photocleavage on DNA. J Photochem Photobiol. 2006; 177:286-294.

44. Svensson FR, Abrahamsson M. Stromberg N, Ewing AG, Lincoln P. Ruthenium(II) Complex Enantiomers as Cellular Probes for Diastereomeric Interactions in Confocal and Fluorescence Lifetime Imaging Microscopy. J Phys Chem Lett. 2011; 2:397-401.

45. Pena B, David A, Pavani C, Baptista MS, Pellois JP, et al. Cytotoxicity studies of cyclometallated ruthenium (II) compounds: new applications for ruthenium dyes. Organometallics. 2014; 33:1100-1103.